Translational

Spontaneous CNV in a Novel Mutant Mouse Is Associated With Early VEGF-A–Driven Angiogenesis and Late-Stage Focal Edema, Neural Cell Loss, and Dysfunction

Norihiro Nagai,[1] Pete Lundh von Leithner,[1] Kanako Izumi-Nagai,[1] Brett Hosking,[1] Bo Chang,[2] Ron Hurd,[2] Peter Adamson,[3] Anthony P. Adamis,[4] Richard H. Foxton,[1] Yin Shan Ng,[1] and David T. Shima[1]

[1]Department of Ocular Biology and Therapeutics, University College London, Institute of Ophthalmology, London, United Kingdom
[2]The Jackson Laboratory, Bar Harbor, Maine, United States
[3]GSK Ophthalmology, GlaxoSmithKline, Stevenage, Hertfordshire, United Kingdom
[4]Genentech, Inc., South San Francisco, California, United States

Correspondence: David T. Shima, UCL Institute of Ophthalmology, 11-43 Bath Street, London, EC1V 9EL; d.shima@ucl.ac.uk.

Submitted: January 20, 2014
Accepted: April 25, 2014

Citation: Nagai N, Lundh von Leithner P, Izumi-Nagai K, et al. Spontaneous CNV in a novel mutant mouse is associated with early VEGF-A driven angiogenesis and late stage focal edema, neural cell loss, and dysfunction. *Invest Ophthalmol Vis Sci*. 2014;55:3709–3719. DOI:10.1167/iovs.14-13989

Purpose. Characterization of a mouse model of spontaneous choroidal neovascularization (sCNV) and its effect on retinal architecture and function.

Methods. The sCNV mouse phenotype was characterized by using fundus photography, fluorescein angiography, confocal scanning laser ophthalmoscopy (SLO), optical coherence tomography (OCT), ERG, immunostaining, biochemistry, and electron microscopy. A role for VEGF-A signaling in sCNV was investigated by using neutralizing antibodies and a role for macrophages explored by cell-depletion studies.

Results. The sCNV starts between postnatal day 10 and 15 (P10–P15), increasing in number and severity causing RPE disruption and dysfunction. Various morphological methods confirmed the choroidal origin and subretinal position of the angiogenic vessels. At approximately P25, vessels were present in the outer retina with instances of anastomosis of some sCNV lesions with the retinal vasculature. The number of CNV lesions was significantly decreased by systemic blockade of the VEGF-A pathway. Choroidal neovascularization size also was significantly modulated by reducing the number of lesion-associated macrophages. Later stages of sCNV were associated with edema, neuronal loss, and dysfunction.

Conclusions. The sCNV mouse is a new model for the study of both early and late events associated with choroidal neovascularization. Pharmacological reduction in sCNV with VEGF-A antagonists and an anti-inflammatory strategy suggests the model may be useful for investigating novel targets for treating human ocular neovascular disease.

Keywords: animal models, neovascularization, VEGF-A

The transformative nature of recent therapeutic developments for neovascular age-related macular degeneration (nAMD) has triggered an exponential increase in ophthalmic drug development efforts over the past decade.[1] The most prevalent assay used to benchmark potential new nAMD compounds and therapeutic strategies is rodent laser-induced choroidal neovascularization (lCNV).[2–5] This model is used to assess antiangiogenic activity and the ability to reduce vascular permeability, two hallmarks of nAMD. Moreover, because of the ease of imaging the posterior pole, lCNV is often used as a secondary pharmacology model during drug development for other conditions, such as cancer. However, the lCNV model has several limitations, including acute, intense laser injury to the photoreceptors, RPE, and choriocapillaris to induce angiogenesis, the accumulation of hypertrophic scar tissue, and a natural regression of the neovascularization.[6] Therefore, factors that initiate the CNV, and long-term analysis of the consequences of the neovessels to the retina, cannot be readily studied. Here we describe a novel genetic model of multifocal, bilateral spontaneous choroidal neovascularization (sCNV), which leads to early, persistent neovascular lesions that leak and lead to retinal edema, local gliosis and focal photoreceptor dysfunction, and death. Approximately 10% to 15% of the lesions will eventually anastomose with the retinal vasculature. As with nAMD in humans, the precise trigger for the neovascularization is unknown, but growth of the lesions and their leakage is driven by VEGF-A, as well as a local parainflammatory response.[7,8] The sCNV model will facilitate an analysis of early local morphological and cellular changes that precede CNV, provide an opportunity for genetic mapping to identify the root cause, and enable longer-term studies to better understand the consequences of CNV to retinal architecture and function.

Methods

Animals

The spontaneous mutant JR5558 line was discovered at The Jackson Laboratory (Bar Harbor, ME, USA). The strain carries the rd8 mutation, but is wild-type for both rd1 (Pde6brd1) and the cone photoreceptor function loss 3 (Gnat2cpfl3) mutations

commonly found in laboratory animals. The strain does not manifest a typical rd8 phenotype, which is suppressed in the C57BL/6J background of the JR5558 strain. The strain was subsequently established at University College London (UCL), where they and age-matched wild-type controls (C57BL/6J, vendor ID 0038, from Charles River Lab, Margate, UK) received food and water ad libitum, in a 12-hour day-night cycle, temperature-controlled environment. When required, mice were anesthetized by intraperitoneal (IP) injection of xylazine (0.5 mg/kg) and ketamine (100 mg/kg) in water. Pupils were dilated with phenylephrine hydrochloride 2.5% and tropicamide 1% (Bausch and Lomb, Surrey, UK) before in vivo imaging. Animal experiments were conducted in accordance with Home Office guidelines (http://goo.gl/FLkirW, last accessed January 2014) and the ARVO Statement for the Use of Animals in Ophthalmic and Vision Research (http://goo.gl/4LFOjD, last accessed January 2014).

Treatment Protocols

To analyze the role of VEGF-A signaling, mice were treated IP with a VEGF receptor (VEGFR)-2 blocking (MAB4431, 25 or 100 μg; R&D Systems, Abingdon, UK) or isotype IgG2a antibody (R&D Systems) daily from postnatal day (P)14 to P24, then CNV development was analyzed by fluorescein angiography[9] on P25. Alternatively, sCNV mice were treated IP with VEGF-A neutralizing antibody (B20.4.1.1; 5 mg/kg; Genentech, San Francisco, CA, USA) or IgG2a control every other day from P14. Fluorescein angiography (FA) was performed on P26.

For the macrophage depletion, sCNV mice were IP injected with clodronate or control liposome (250 mg; Encapsula NanoSciences, Nashville, TN, USA) from P8 to P18, every other day. Choroidal neovascularization development was analyzed by immunostaining with FITC-conjugated isolectin B4 on P19 eyes.

In Vivo Imaging

Fundus photography and retinal angiography were performed on conscious mice as previously described.[10] Lesion number and area were quantified using ImageJ (http://imagej.nih.gov/ij/; provided in the public domain by the National Institutes of Health, Bethesda, MD, USA). Lesion area is represented in most figures as percentage of control; however, statistics were done on raw pixel measurements.

Optical coherence tomography (OCT) and confocal scanning laser angiography were done using a Heidelberg Spectralis (Heidelberg Engineering GmbH, Heidelberg, Germany) on anesthetized mice. For angiography, the device was operated in standard fluorescence mode (FA at 488/498 nm).

An achromatic ±25-diopter doublet lens adapted the OCT to mouse eyes. Adjacent 30° field-of-view 1536 × 1536 pixel (px) B-scans were recorded at 10-μm intervals. A software algorithm (Matlab; Mathworks, Inc., Natick, MA, USA) extracted the boundary separating the outer segment layer from the subretinal space, and the apical surface of the RPE from the OCT 3-dimensional (3D) data volumes, based on Koprowski et al 2008.[11] Topographic maps were generated showing subretinal space thickness variations.

Perfusion Assays

Under deep anesthesia, Sulfo-NHS-Biotin (250 μg; Thermo Fisher Scientific, Waltham, MA, USA) was injected intracardially, followed either after 10 seconds (retinal section), or 1 minute (whole-mount RPE-Choroid complex) by PBS and 4% paraformaldehyde (PFA). Eyes were enucleated and prepared as frozen sections or wholemounts (see below). Tissues were counterstained with Alexa Fluor 594 conjugated Streptavidin (Invitrogen, Paisley, UK) and 4′,6-diamidino-2-phenylindole (DAPI).

Concanavalin A leukostasis was performed as described.[12] Under deep anesthesia, the mouse was cardiac perfused with rhodamine-conjugated concanavalin A (Rho-Con A; Vector Laboratories, Peterborough, UK), followed by PBS. Eyes were fixed in 4% PFA for 1 hour at room temperature (RT), then retinas wholemounted in Vectashield (Vector Laboratories). Leukocytes inside vessels of the entire retina were counted under epifluorescence microscopy.

Electroretinography

Standard scotopic and photopic large-field ERGs were recorded from dark- (12 hours) and light-adapted mice (Micron III; Phoenix Research Laboratories, Pleasanton, CA, USA). Scotopic recordings were performed under dim red light. Series of 5-ms single-flash recordings were obtained at increasing light intensities from −2.5 to 3.0 log cds/m^2. Twenty responses per intensity were averaged with an interstimulus interval of 20 seconds. The a- and b-wave amplitudes and implicit times were evaluated (Labscribe; iWork System, Inc., Dover, NH, USA).

Histology and Immunostaining

Eyes were fixed in 4% PFA for 2 to 8 hours at RT and prepared as wholemounts, or transverse sections. For sections, eyes were cryoprotected in 30% sucrose, snap-frozen in optimum cutting temperature compound (TissueTek; Sakura Finetek, Thatcham, UK) and cryostat sections (10 μm) thaw-mounted onto glass slides. Tissue was blocked for 1 hour with 1% bovine serum albumin or 10% normal goat serum, then permeabilized in 0.3% Triton X-100 (sections), or 3.0% Triton X-100 (wholemounts), and incubated with primary antibodies (see Table) in blocking solution overnight at 4°C. Secondary antibodies were applied for 1 (sections), or 2 hours (wholemounts) at RT and stained with DAPI. After final washes the tissue was coverslipped in Vectashield.

A terminal dUTP nick end-labeling (TUNEL) assay was performed on retinae (sections and wholemounts) according to the manufacturer's protocol (Promega, Southampton, UK). TUNEL-processed tissues were counterstained with PECAM-1 antibody, or isolectin-IB4. The number and position of TUNEL-positive cells was recorded.

Outer nuclear layer (ONL) thickness was measured in sections of the entire retina along the optic nerve that were stained with hematoxylin and eosin (H&E; Sigma-Aldrich, Dorset, UK). The thickness of the ONL was measured at four uniformly distributed locations along a radius from the center of the optic nerve head to ora serrata.[13]

Antibodies for Immunostaining

Primary antibodies and stains are listed in the Table.

Microscopy

Bright-field and epifluorescence was performed using an Olympus BX51 microscope (Olympus, Essex, UK) with a Retiga SRV camera (QImaging, Surrey, BC, Canada).

Confocal microscopy was done on a Zeiss LSM 700 or 710 (Carl Zeiss Ltd., Cambridge, UK).

Serial block-face scanning electron microscopy was performed as described previously[15] with modifications.[16] Briefly, regions of interest were cut from resin blocks, sputter coated

TABLE. Primary Antibodies and Stains

Name	Type	Company	Code	Dilution
F4/80	mAb	Abcam, Cambridge, UK	AB 6640	1:200
GFAP	pAb	DAKO, Ely, UK	ZO334	1:400
CD31 (PECAM-1)	pAb	BD Biosciences, San Diego, CA	BD 553370	1:500
ZO-1	mAb (rabbit)	K.M., UCL*		1:400
Fluorescein-labeled GSL I-B_4 isolectin	Lectin stain	Vector Laboratories	FL-1205	1:400
EZ-Link Sulfo-NHS-LC-Biotin	Avidin-Biotin stain	Thermo Scientific, Loughborough, UK	21327	10 mg/mL

pAb, polyclonal Ab.
* Kindly provided by Karl Matter, PhD.[14]

with 5-nm gold palladium, locked into the ultramicrotome (3View; Gatan UK, Ltd., Oxon, UK), and mounted to a Sigma variable pressure field emission scanning electron microscope (Carl Zeiss Ltd.). Image stacks spanning 99 μm at 4096 × 4096 px were acquired. Three-dimensional reconstruction and labeling was obtained using Amira 5.3.3 software (Visage Imaging, Inc., Berlin, Germany).

Protein Analysis

For ELISA, retina and RPE/choroid complex were harvested into RIPA lysis buffer (Sigma-Aldrich), supplemented with protease inhibitors and sonicated. The lysate was centrifuged at 22,000*g* for 10 minutes at 4°C and VEGF-A levels in the supernatant were determined with ELISA kits (R&D Systems, Minneapolis, MN, USA) according to the manufacturer's protocol. The tissue sample concentration was calculated from a protein standard curve.

Statistics

All results were expressed as mean ± SEM unless otherwise indicated. Statistical significance was calculated using a Student's *t*-test, or for three or more comparisons one-way ANOVA followed by Newman-Keuls post hoc comparisons. Differences were considered statistically significant at P less than 0.05.

RESULTS

sCNV Development and Early Morphological Changes

The JR5558 mouse (The Jackson Laboratory) harbors recessive mutations in unknown genes, which in the homozygous state, leads to numerous neovascular tufts originating from the choriocapillaris in the center to midperiphery of the fundus between P10 and P15 (Fig. 1). The phenotype is more than 95% penetrant, is not influenced by sex, and nonocular phenotypes have not been observed. By fluorescein angiography,[9] the lesions were visible within 90 seconds of IP administration of sodium fluorescein, with leakage continuously increasing thereafter. By fundus color photography, the lesions were associated with multifocal pigmentary changes, but the neovasculature could not be observed (Fig. 1A). Immunostaining of eyecups devoid of the retina using a vascular marker enabled more quantitative analyses and revealed that sCNV lesions increase in number and size with age (Fig. 1B). The number of lesions peaks at 15 to 20 per eye at approximately P30, and after this time point some individual lesions coalesced into larger lesions (Fig. 1C). Immunostaining, tracer studies, and histology all confirmed that the early lesions originated from, and were contiguous with the choriocapillaris, and they disrupted the RPE (Figs. 2A–C, Supplementary Figs. S1A, S2A). Electron microscopic images show that most CNV lesions grow and occupy the subretinal space, either apical to, or embedded within the RPE layer (Fig. 2D, Supplementary Fig. S3). Confocal imaging with a focus on the choriocapillaris-RPE interface revealed the accumulation of single cells positive for endothelial markers along the choriocapillaris vascular bed at P10 (Figs. 3A–C). Small endothelial cell sprouts emanating from the RPE layer also appeared at P10, with the pioneer cells rich in filopodia (Figs. 3D–F). Concordantly, the early choroidal vessel invasion is associated with changes in RPE phenotype, including depigmentation (Figs. 1A, 2C), focal loss of ZO-1 expression, and disruption of RPE barrier function (Supplementary Fig. S1). After P20 to P25, confocal imaging revealed that approximately 10% to 15% of the sCNV lesions grow into the ONL and anastomose with the deep retinal vascular plexus ($n = 20$ eyes; Figs. 3G, 3H).

VEGF-A Is Required for sCNV

A role for VEGF-A in sCNV was investigated to determine if the mouse model mimics one of the key aspects driving human CNV.[17] First, VEGF-A levels were quantified by ELISA in the choroid/RPE complex and the retina. Vascular endothelial growth factor-A was elevated in both tissues during the time of CNV growth, between P10 and P21 (Figs. 4A, 4B). Blockade of VEGF-A with a neutralizing mAb from P14 to P24, a period chosen because it represents the time of peak sCNV growth, demonstrated that the average number and size of CNV lesions were significantly reduced (Fig. 4C). Vascular endothelial growth factor receptor 2 signaling is believed to be the main pathway involved in pathological ocular angiogenesis,[18] and administration of a VEGFR2 neutralizing antibody confirmed that it plays a significant role in VEGF-A–mediated sCNV (Fig. 4D).

Para-Inflammation Is an Important Factor in sCNV Growth

It has previously been suggested that para-inflammation, a local tissue response to injury or stress, may contribute to ocular neovascularization in humans,[19] as well as in animal models.[20] Macrophages are present in CNV lesions, and depletion of these using various means reduces CNV lesion size.[21] We probed the role of the macrophage in the sCNV model, first examining the adherent leukocytes in the retinal vasculature, by perfusion-labeling with Rhodamine-Con A. Leukocyte counts were significantly increased in sCNV compared with the age-matched controls (57.4 ± 6.3 cells/retina versus 5.0 ± 0.61 cells/retina, $n = 4$, $P < 0.05$). Next, we analyzed the infiltration of macrophage in sCNV. F4/80 immunostaining revealed that at an early stage of CNV development (P10), there were occasional F4/80-positive macrophages associated with the small neovascular tufts. Later the development of all individual sCNV lesions was accompanied by closely associated

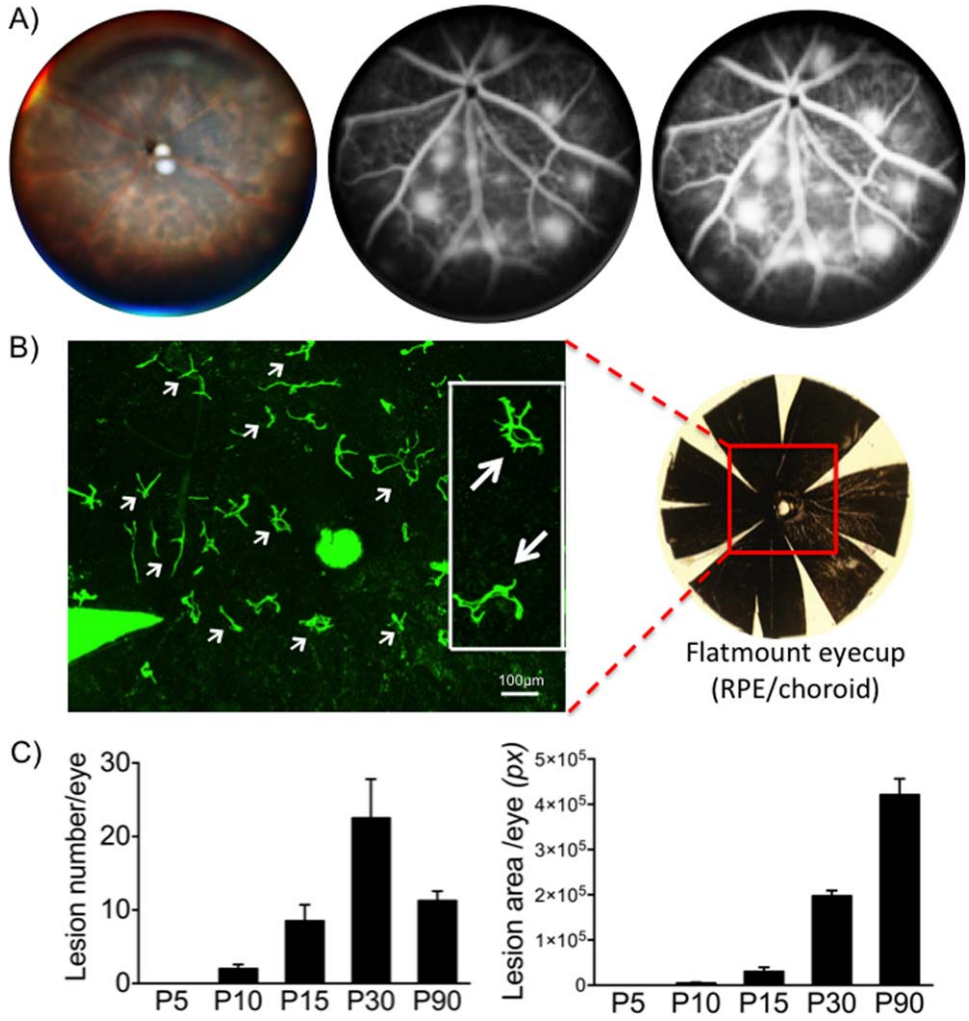

Figure 1. Spontaneous CNV and early morphological changes in the posterior segment of the sCNV mouse eye. (**A**) Fundus image illustrating focal pigmentation changes at the RPE level (*left*), alongside fluorescein angiographs showing subretinal CNV lesions at 1.5 (*middle*) and 5.0 minutes (*right*) after 2% fluorescein administration. (**B**) *Left*: Isolectin-B4 staining (*green*) of RPE/choroid flatmounts (retina removed) revealing neovascular tufts at low (*small arrows*) and higher magnification (*white box*; *larger arrows*). *Right*: An eyecup showing the area of interest. (**C**) Number of CNV lesions (*left*) and lesion area per eye in pixels (*right*) from P5 to P90 animals ($n = 4$ for all).

F4/80-positive macrophages (Fig. 5A). To investigate if macrophages were involved in the formation of sCNV, mice were systemically treated with clodronate liposomes, which leads to a depletion of blood monocytes and lymph node macrophages in the mouse.[22] Reduction in F4/80-positive macrophages was confirmed by immunostaining, and resulted in a decrease in lesion size, but not number (Fig. 5B). These data suggest that macrophages are involved in driving the growth of existing CNV, rather than initiating vessel growth. The data are consistent with our earlier observation, that as initial vascular sprouts were invading the subretinal space, the presence of F4/80-positive macrophages was variable; therefore, macrophages are not a strict requirement for CNV. Also in support was the morphology of the CNV lesions following clodronate treatment, with the subretinal vessels often appearing as single sprouts, rather than large globular lesions (Figs. 3A, 5B). Finally, we observed that clodronate treatment was not completely effective and there were examples where 1 to 2 sCNV lesions out of the total 15 to 20 within an eyecup would still be associated with macrophages, and these lesions were significantly larger (data not shown).

Later Stages of sCNV Associated With Edema and Focal Neuro-Glial Dysfunction and Photoreceptor Loss

Unlike lCNV, which begins to retreat 7 to 10 days post laser,[6] sCNV lesions are present for at least 3 months (no observations made beyond this time point). This enables one to explore both the morphology and the consequences of advanced sCNV lesions on retinal ultrastructure and function at various time points from P40 to P90. Using OCT, we observed areas of low reflectivity (arrows) in the outer retina delineating fluid-filled regions that encircled sCNV lesions (arrowheads). Topographic maps of OCT data demonstrated areas of subretinal elevation, the majority associated with CNV lesions that colocalized with leakage in FA (Figs. 6A–C). Vascular permeability tracer studies and angiography both demonstrated that there was increased permeability of the neovasculature, which over time, could lead to accumulation of retinal or subretinal fluid, and explain the OCT findings (Figs. 2A, 2B, 6). Use of serial section electron microscopy provided data in support of fluid accumulation. Proximal to intra-RPE or subretinal neovessels appeared as cyst-like structures, and higher magnifica-

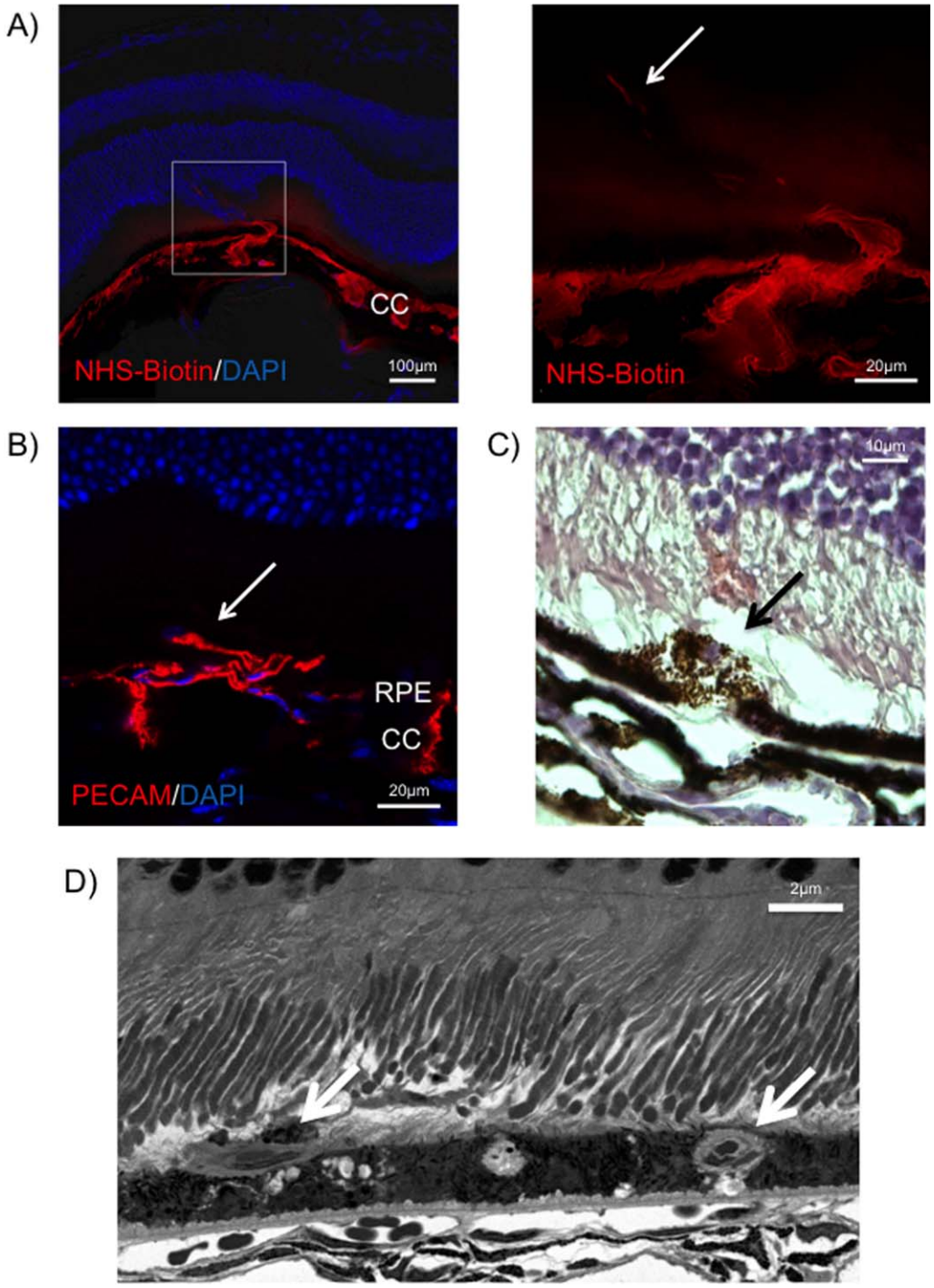

FIGURE 2. Choroidal origin of neovascular tufts in sCNV mice. (**A**) Small molecular weight tracer (NHS-biotin, *red*) study showing continuous labeling and perfusion of the choriocapillaris (CC) (*left*, low magnification), as well as the sub-retinal CNV (*right*, higher magnification, *white arrow*) 10 seconds after tracer injection in P20 mice. Note leakage of tracer from the CNV into the outer retina. (**B**) PECAM staining reveals continuity of CNV and choriocapillaris (*white arrow*). (**C**) Hematoxylin and eosin staining demonstrating disruption of Bruch's membrane and the RPE layer by the CNV (partly visible in section; *black arrow*. See also Supplementary Fig. S2). (**D**) Ultrastructural image from P20 mouse of neovessels in the subretinal space as well as within the RPE layer (*white arrows*).

tion observations of the RPE were consistent with fluid accumulation (Fig. 6C). However, the composition of the cysts and the basis of the OCT findings will require further study to elaborate on these initial findings.

The disruption of normal RPE function, the cyst-like structures separating the RPE and photoreceptors, and the presence of neovessels are likely to eventually lead to outer retina damage. Progressive retinal degeneration and dysfunction have been observed in patients with neovascular AMD.[23,24] Glial fibrillary acidic protein (GFAP) is an established indicator of retinal stress and is upregulated in a number of retinal disorders, including AMD, diabetic retinopathy, retinal detachment, and ischemia.[25] In sCNV retinae, GFAP was upregulated proximal to areas of CNV; moreover, the large

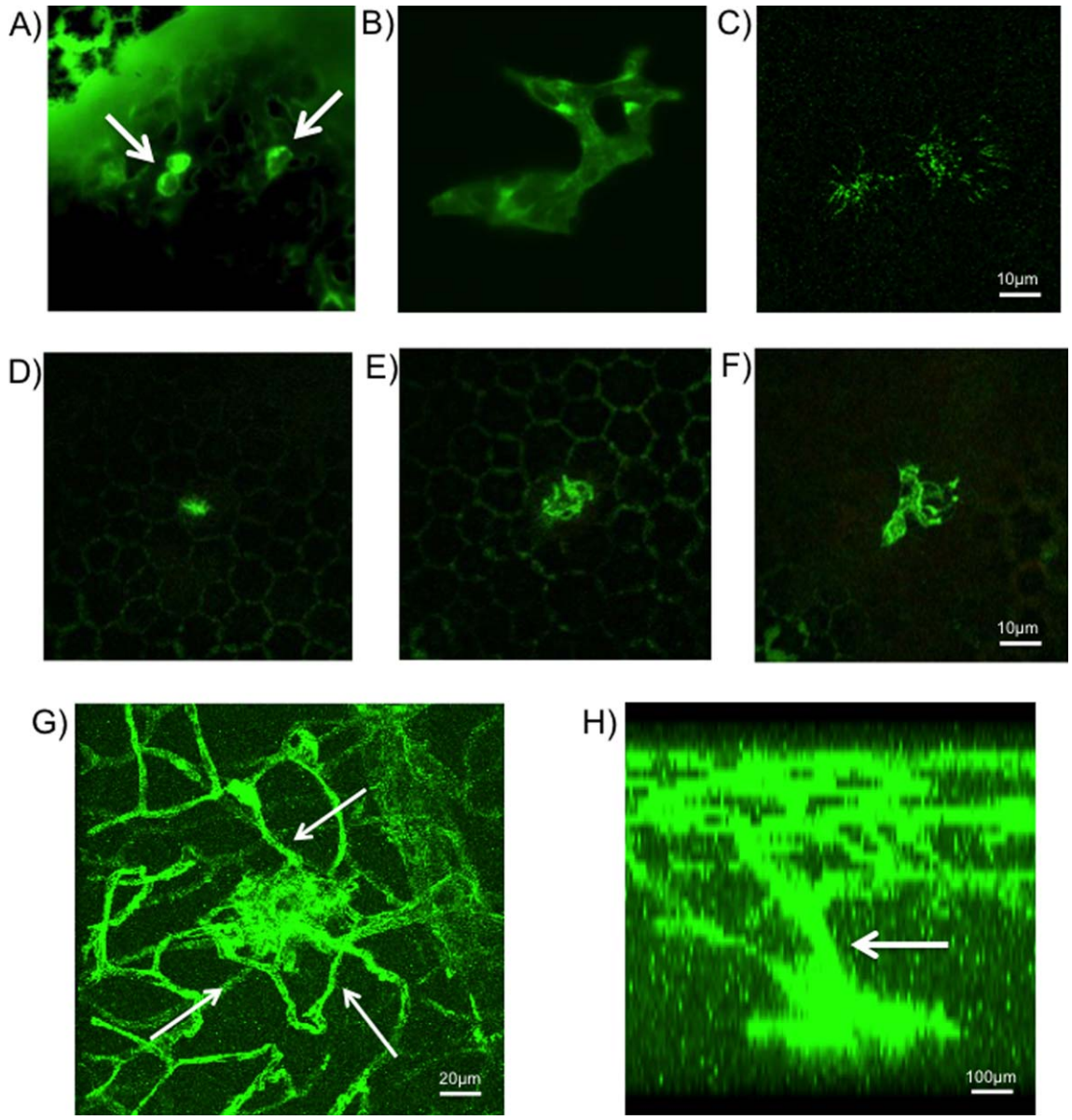

FIGURE 3. Early vascular changes in the choriocapillaris and subretinal and retinal space. (**A**) At P10, confocal images of isolectin-B4 (*green*) staining between the choriocapillaris and RPE, show an accumulation of individual cells (*white arrows*) and (**B**) primitive neovascular sprouts, with (**C**) endothelial tip cells rich in filopodia. (**D–F**) Three consecutive confocal images of a neovascular sprout (isolectin-B4, *green*) emerging through the polygonal green autofluorescent RPE layer. (**G**) Vascular stain (isolectin-B4, *green*) at P25 shows an anastomosis (*white arrows*) of the CNV with the deep retinal vascular plexus. (**H**) A 3D confocal microscopy reconstruction of the vascular anastomosis (*white arrow*).

accumulation of GFAP-positive glia also suggested ongoing gliosis (Fig. 7A).

To understand the impact on the photoreceptors, the thickness of the ONL of P20, P30, and P60 sCNV mice was measured. At P30 and P60, the ONL was significantly thinner than that of age-matched wild-type mice in the posterior retina, where most CNV occurs (Fig. 7B). TUNEL staining of sCNV retinas showed an increase in apoptotic photoreceptor nuclei, with very few TUNEL-positive cells observed in the inner retina (Figs. 7C, 7D). Like the GFAP expression, TUNEL-positive cells were primarily located proximal to CNV lesions (Figs. 7D, 7E). Finally, as expected, the stress and general demise of retinal cells led to a decrease in visual function. Electroretinography was used to assess retinal function in response to large-field flash stimuli under both scotopic and photopic conditions. Large-field ERGs demonstrated reproducible delay and depression in both scotopic and photopic b-wave amplitude in sCNV mice compared with age-matched controls (Fig. 7F).

DISCUSSION

The advent of anti–VEGF-A therapy has shifted focus for many AMD researchers to the events upstream and downstream of neovessel formation. The trigger for angiogenesis, and the precise consequences of CNV for neural survival and function are still poorly understood. Here we describe a mouse model that could provide new insight into CNV pathobiology and potentially, novel drug targets.

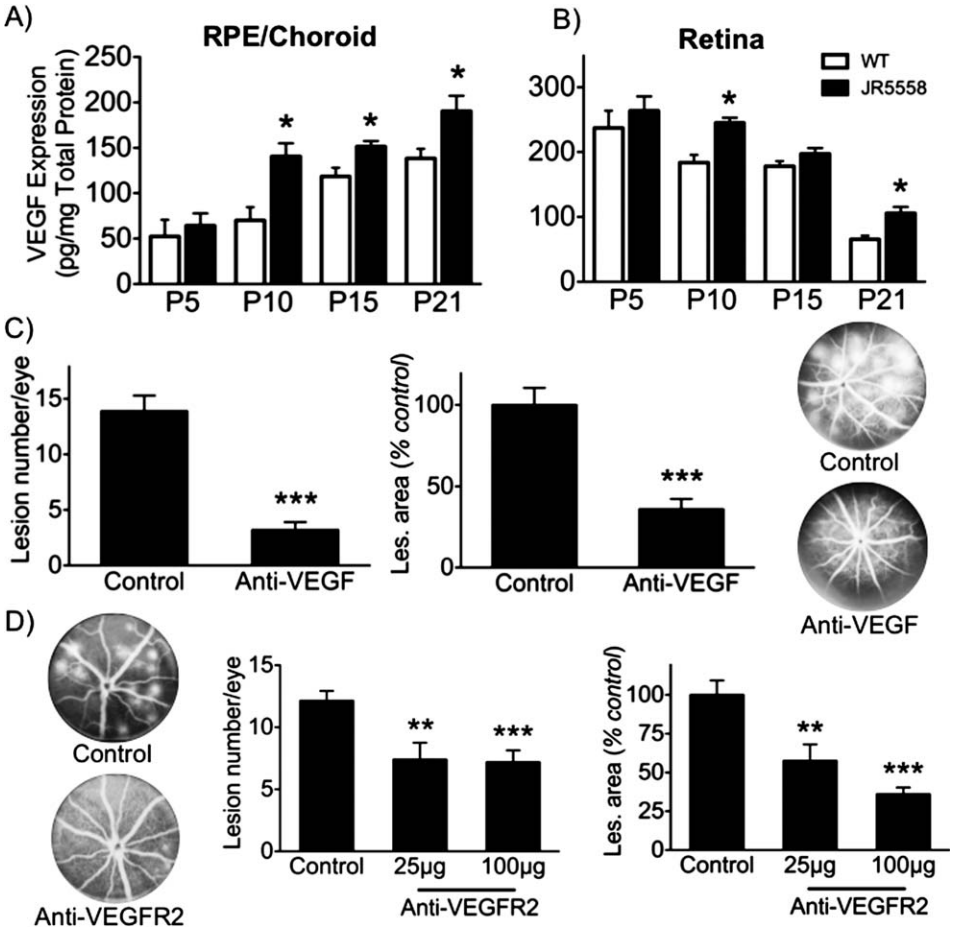

FIGURE 4. Critical role of VEGF-A in spontaneous CNV development. (**A**) Protein levels of VEGF-A in the RPE/choroid (*left*), and (**B**) retina (*right*) during postnatal eye development. Vascular endothelial growth factor-A was significantly higher in sCNV versus age-matched C57/Bl6 ($n = 6$–8). (**C**) Vascular endothelial growth factor-A antagonism significantly reduced CNV lesion number (*left*) and area (*right*) per eye ($n = 13$–15), with representative fundus fluorescein angiograms (FFA) from control and anti-VEGF–treated eyes. (**D**) Vascular endothelial growth factor receptor 2 neutralizing antibody also significantly diminished both the average CNV number (*left*) and area (*right*) per eye ($n = 20$), with representative FFA images on the left. $^{*}P < 0.05$; $^{**}P < 0.01$; $^{***}P < 0.005$.

Choroidal Neovascularization

Other mouse models of subretinal and CNV have been described. For example, growth factors such as basic FGF and VEGF-A have been injected subretinally to trigger CNV.[26] Schwesinger et al.[27] overexpressed VEGF-A in the RPE, which led to intrachoroidal neovascularization. More recently, a very low-density lipoprotein receptor (VLDLR) knockout mouse was described that exhibited subretinal neovascularization,[28] but it is now believed that the neovessels are of retinal origin.[29] Although the mouse strains are distinct, we did investigate if the sCNV mouse had a similar upregulation of Wnt signaling, which was shown to drive the neovascularization in the VLDLR knockout mouse.[30] However, in contrast to these mice, no changes to β-catenin protein or phosphorylation were observed in the JR5558 mouse (Nagai N, unpublished data, 2012), which suggests a distinct disease mechanism underpins the CNV.

The disease process in the JR5558 strain started early and appeared to originate in the choroid. Groups of endothelial cells and primitive vascular structures appeared between the RPE and choriocapillaris from P10 to P15. Vascular sprouts were directed toward the RPE, were rich in filopodia, and by P15 were readily observed sprouting through the RPE layer into the subretinal space. Vascular endothelial growth factor-A appeared to be an important driver of the early angiogenic sprouting, as blockade decreased the number of CNV lesions. Interestingly, depletion of systemic and local macrophages had no effect on lesion number, suggesting that their role was to drive the growth of existing CNV, rather than trigger the early angiogenesis in the sCNV mouse. However, we cannot rule out that the clodronate approach used to deplete macrophages could be affecting other cell types; therefore, more specific targeting of different macrophage subtypes using pharmacological or genetic approaches will be required to confirm our findings.

Although there are very few clinically confirmed targets for nAMD, the validation of VEGF-A as a driver for CNV and its associated vascular leakage in the sCNV model suggests that findings in this model might be translatable to the human condition. If true, the sCNV model will be a valuable tool for testing of novel drug candidates for human CNV. Additionally, the observation that there is some anastomosis of the CNV with the retinal circulation provides an opportunity to explore a pathobiology that may offer insight into the human condition of retinal angiomatous proliferation.[31] The mechanisms responsible for the sporadic anastomoses will be an interesting focus for further work.

One clear limitation of the sCNV mouse is that the CNV does not occur within an aging eye or in an AMD-like context

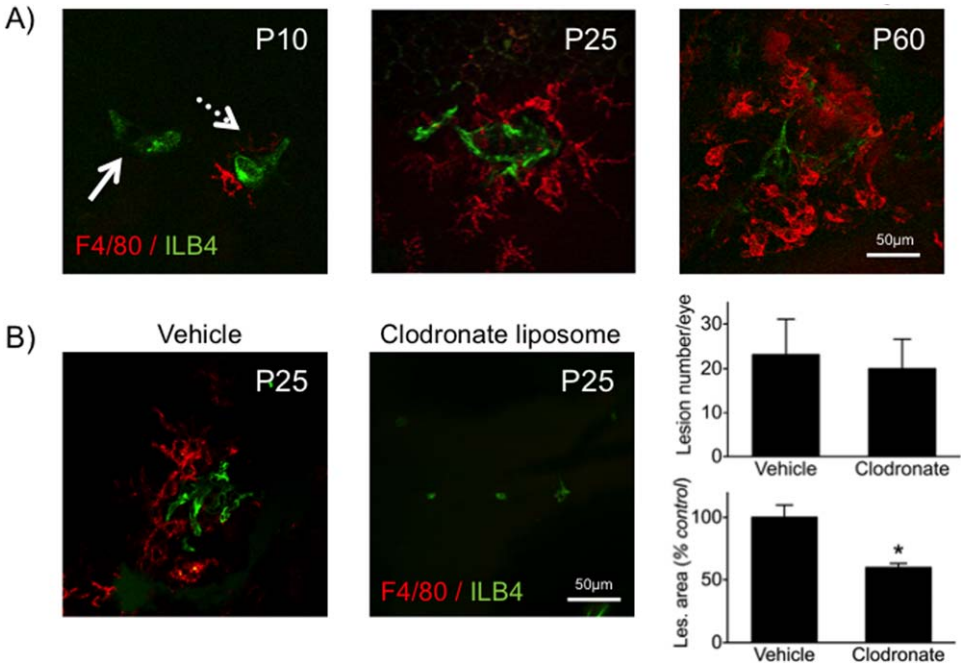

Figure 5. The role of para-inflammation in CNV growth. (**A**) Immunohistological analysis of F4/80-positive macrophage recruitment to subretinal neovascular lesions (isolectin B4, *green*) at early-stage CNV (*left*, P10); with (*dotted arrow*) and without (*solid white arrow*) associated macrophages. As the CNV grew, macrophage association increased (*middle*, P25, and *right*, P60). (**B**) F4/80 staining showing reduction in CNV size (isolectin B4, *green*) and macrophage number in the clodronate liposome-treated group (*middle*), compared with vehicle-treated animals with larger CNV lesions, and numerous F4/80-positive macrophages (*left*). Monocyte depletion by clodronate liposomes significantly reduced CNV area, but not number per eye (*right*). $n = 4$–6, $^*P < 0.05$.

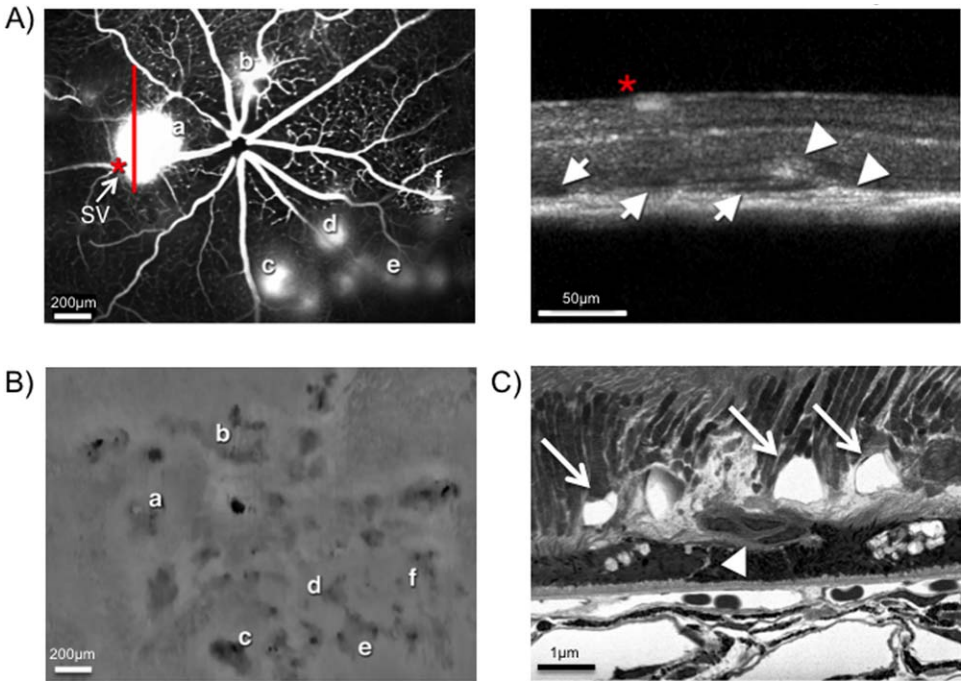

Figure 6. Evidence of edema in later stages of spontaneous CNV. (**A**) *Left*: Fluorescein angiogram showing a large CNV lesion with increased permeability and the location for OCT line scanning (*red line*). *Right*: OCT image of the lesion shown in *left image* demonstrating low reflectivity (*arrows*) in the outer retina delineating fluid-filled regions that encircled sCNV lesions (*arrowheads*). *Red asterisk* indicates the same superficial vessel in *left* and *right images*. (**B**) Maximum-intensity projection of OCT data from the same sample, illustrating areas of outer-retinal elevation (*darker grey*). Note correspondence of CNV leakage (from [**A**]) with many of the areas of elevation (**a**–**f**). (**C**) Ultrastructural image of the retina/RPE/choroid interfaces showing cystic-like structures (*arrows*) in the subretinal space near the established CNV (*arrowhead*). All images are from P40 eyes. SV, superficial vessel.

Investigative Ophthalmology & Visual Science

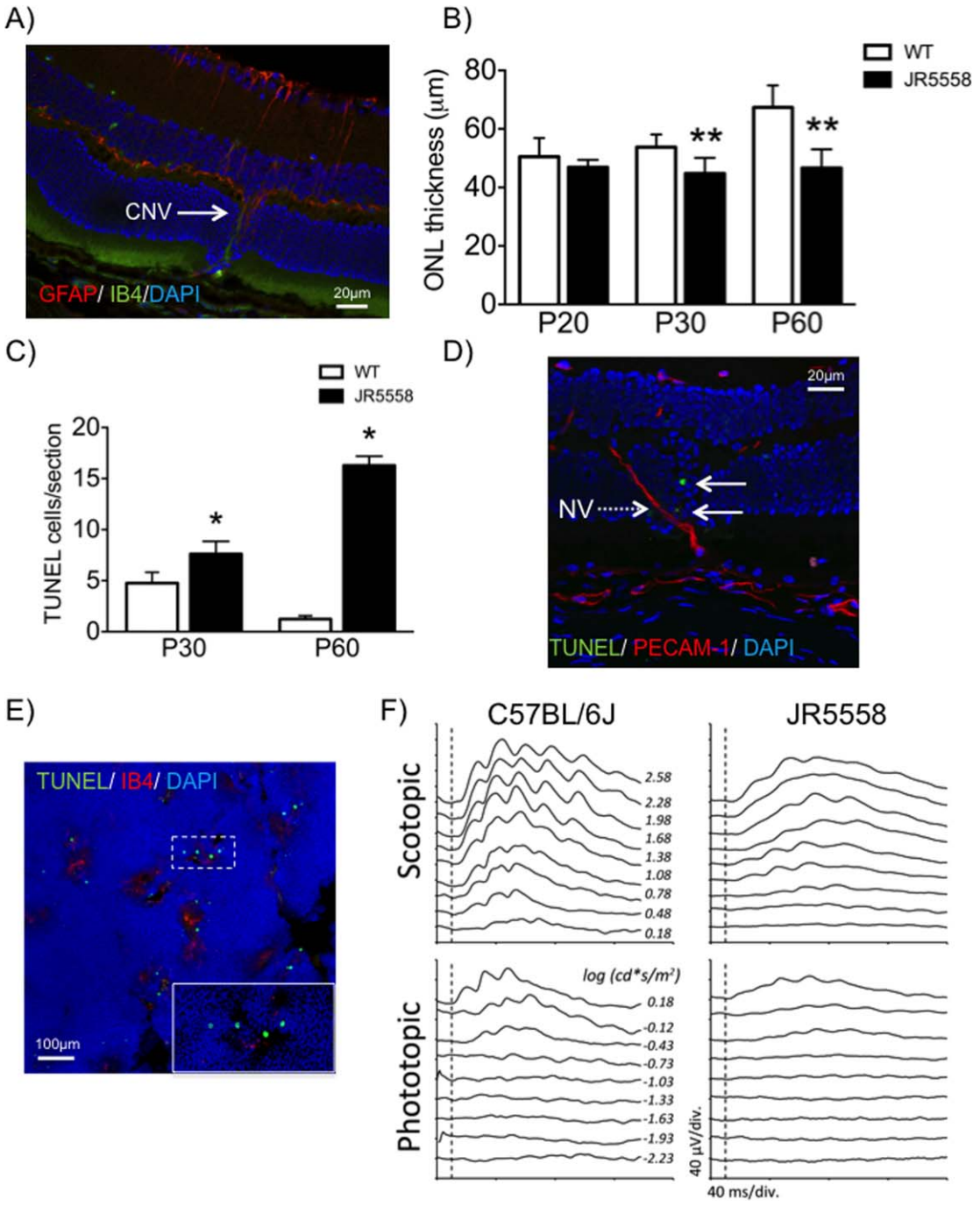

Figure 7. Glial fibrillary acidic protein upregulation and focal retinal degeneration in the sCNV mouse. (**A**) Glial fibrillary acidic protein expression is upregulated in retinae (P30), especially around the CNV (*green*). Glial fibrillary acidic protein–positive processes extend from the ganglion cell layer to the CNV. (**B**) Comparison of ONL thickness between sCNV and C57/Bl6 mice, showing thinning in sCNV retinas at P30 and P60 ($n = 6$). (**C**) Elevated apoptosis (TUNEL staining) was detected in the sCNV retina at both P30 and P60 compared with C57/Bl6 ($n = 6$–7). TUNEL staining of a retinal section (**D**) and whole mount (**E**) at P60 showing TUNEL-positive photoreceptor nuclei (*green*) in the ONL proximal to the CNV (PECAM-1, section; isolectin-B4, whole mount; both *red*). (**F**) Representative ERG flash responses showing a reduction of retinal function of the sCNV mouse in both scotopic and photopic conditions. $n = 4$, $^{*}P < 0.05$, $^{**}P < 0.01$.

(drusen and other deposits). However, because the underlying triggers of CNV are largely unknown, studying the spontaneous local changes that accompany the neovascularization (pigmentary changes, alteration of RPE barrier control, breaching of the outer retinal barrier by vessels) may provide novel insight beyond that provided by breaching the barrier with a laser. From a more practical point of view, the sCNV model requires no surgery or laser use, reducing both costs and variability between operators.

Additional Chorio-Retinal Changes

Accompanying the CNV in the model were alterations that might have been expected, such as fractures in the RPE layer and changes to RPE phenotype, including loss of pigment.

However, we also had surprising findings, such as the widespread loss of expression of the junctional protein ZO-1, and loss of RPE barrier function observed in the tracer studies. These changes were not restricted to CNV regions, but were prevalent throughout central retinae. The cause of this is unknown, but could be part of the mutant mouse phenotype, and thereby may facilitate the sCNV. For example, loss of differentiated function may lead to changes in polarity and the apical secretion of VEGF-A, which is normally secreted basolaterally.[32] This could in turn act as an attractant for the choriocapillaris to grow into the subretinal space. The compromise of the RPE barrier and the leakage of the CNV are likely to contribute to the apparent edema observed in the subretinal space. Optical coherence tomography imaging demonstrated large areas of retinal elevation around the periphery of the CNV. By electron microscopy, cystic-like structures were observed apical to the RPE, and very large vacuoles were present within the RPE. Persistent retinal or subretinal fluid has not been described for rodent CNV models, and if indeed this were subretinal fluid, it would be a unique and valuable feature of the sCNV model. One would have both the ability to study the contribution of vascular permeability, but importantly, also the loss of the outer blood-retinal barrier function of the RPE. Additionally, therapeutic strategies focused on tightening the RPE barrier can be investigated.

Independent of the precise composition of the large cystic-like structures apical to the RPE, the disruption of the normal and essential photoreceptor outer segment–RPE interface is likely to have an adverse effect on photoreceptor function. Indeed, focal photoreceptor death, gliosis, and depressed b-wave function were observed in animals with established sCNV. Two important areas of investigation become enabled by these findings. First, the model presents an attractive system for testing strategies aimed at protecting the photoreceptors following CNV. Second, the model presents an opportunity to determine the detailed basis of photoreceptor loss and dysfunction. Is it the presence of vessels in the outer retina, RPE dysfunction, edema, local para-inflammation, or a combination of these abnormalities that lead to the ultimate decline in visual function?

Finally, the sCNV mouse will provide important clues about the genetic risk factors associated with CNV. Although initial genetic exploration suggests complex inheritance patterns and the likelihood of more than one gene defect, eventual mapping of the gene defect(s) should provide mechanistic insight into the pathways that are capable of initiating the angiogenic switch, at least in mouse CNV. In support of this idea, there is increasing evidence to think that there is a reasonable chance of translatability between human genetic findings and mouse genetic and pharmacology models. For example, reduction in complement activation has been shown to reduce the severity of CNV in the mouse laser model[33] in line with the expectations based on human genetics findings in AMD.[34] Also, recent mouse transgene experiments suggest that manipulation of HTRA protein expression may provide insight into the mechanistic basis of the risk associated with the human gene polymorphisms.[35,36] Taken together, the sCNV mouse represents a valuable research tool for disease mechanism studies, as well as drug discovery and development opportunities for CNV associated with AMD.

Acknowledgments

Supported by a multiuser equipment grant from The Wellcome Trust (099173/Z/12/Z), the Medical Research Council (G0800946), the National Eye Institute (Grant EY019943), Jerini Ophthalmic, Genentech, and GlaxoSmithKline. We thank Peter Munro, PhD, for his assistance with microscopy and imaging.

Disclosure: **N. Nagai**, None; **P. Lundh von Leithner**, None; **K. Izumi-Nagai**, None; **B. Hosking**, None; **B. Chang**, None; **R. Hurd**, None; **P. Adamson**, GSK (I, E); **A.P. Adamis**, Genentech (I, E); **R.H. Foxton**, None; **Y.S. Ng**, None; **D.T. Shima**, GSK (F), Jerini Ophthalmic (F), Genentech (F, C, R)

References

1. Kaiser PK. Emerging therapies for neovascular age-related macular degeneration: drugs in the pipeline. *Ophthalmology*. 2013;120:S11–S15.
2. Dobi ET, Puliafito CA, Destro M. A new model of experimental choroidal neovascularization in the rat. *Arch Ophthalmol*. 1989;107:264–269.
3. Pennesi ME, Neuringer M, Courtney RJ. Animal models of age related macular degeneration. *Mol Aspects Med*. 2012;33:487–509.
4. Grossniklaus HE, Kang SJ, Berglin L. Animal models of choroidal and retinal neovascularization. *Prog Retin Eye Res*. 2010;29:500–519.
5. Edwards AO, Malek G. Molecular genetics of AMD and current animal models. *Angiogenesis*. 2007;10:119–132.
6. Kuroki AM, Bhutto IA, Kitaoka T, Amemiya T. Natural course of experimental choroidal neovascularization: three-dimensional study with corrosion cast and scanning electron microscope. *Ophthalmic Res*. 2002;34:200–205.
7. Kwak N, Okamoto N, Wood JM, Campochiaro PA. VEGF is major stimulator in model of choroidal neovascularization. *Invest Ophthalmol Vis Sci*. 2000;41:3158–3164.
8. Oh H, Takagi H, Takagi C, et al. The potential angiogenic role of macrophages in the formation of choroidal neovascular membranes. *Invest Ophthalmol Vis Sci*. 1999;40:1891–1898.
9. Marneros AG, Fan J, Yokoyama Y, et al. Vascular endothelial growth factor expression in the retinal pigment epithelium is essential for choriocapillaris development and visual function. *Am J Pathol*. 2005;167:1451–1459.
10. Robbie SJ, Lundh von Leithner P, Ju M, et al. Assessing a novel depot delivery strategy for noninvasive administration of VEGF/PDGF RTK inhibitors for ocular neovascular disease. *Invest Ophthalmol Vis Sci*. 2013;54:1490–1500.
11. Piñetka E, Kawa J. *Information Technologies in Biomedicine. Advances in Soft Computing*. Berlin: Springer; 2008:xiii, 574.
12. Joussen AM, Murata T, Tsujikawa A, Kirchhof B, Bursell SE, Adamis AP. Leukocyte-mediated endothelial cell injury and death in the diabetic retina. *Am J Pathol*. 2001;158:147–152.
13. Chen Y, Hu Y, Moiseyev G, Zhou KK, Chen D, Ma JX. Photoreceptor degeneration and retinal inflammation induced by very low-density lipoprotein receptor deficiency. *Microvasc Res*. 2009;78:119–127.
14. Benais-Pont G, Punn A, Flores-Maldonado C, et al. Identification of a tight junction-associated guanine nucleotide exchange factor that activates Rho and regulates paracellular permeability. *J Cell Biol*. 2003;160:729–740.
15. West JB, Fu Z, Deerinck TJ, Mackey MR, Obayashi JT, Ellisman MH. Structure-function studies of blood and air capillaries in chicken lung using 3D electron microscopy. *Respir Physiol Neurobiol*. 2010;170:202–209.
16. Luhmann UF, Lange CA, Robbie S, et al. Differential modulation of retinal degeneration by Ccl2 and Cx3cr1 chemokine signalling. *PLoS One*. 2012;7:e35551.
17. Ferrara N. Vascular endothelial growth factor and age-related macular degeneration: from basic science to therapy. *Nat Med*. 2010;16:1107–1111.
18. Meyer M, Clauss M, Lepple-Wienhues A, et al. A novel vascular endothelial growth factor encoded by Orf virus, VEGF-E, mediates angiogenesis via signalling through VEGFR-2 (KDR)

but not VEGFR-1 (Flt-1) receptor tyrosine kinases. *EMBO J*. 1999;18:363–374.

19. Grossniklaus HE, Cingle KA, Yoon YD, Ketkar N, L'Hernault N, Brown S. Correlation of histologic 2-dimensional reconstruction and confocal scanning laser microscopic imaging of choroidal neovascularization in eyes with age-related maculopathy. *Arch Ophthalmol*. 2000;118:625–629.
20. Nishimura T, Goodnight R, Prendergast RA, Ryan SJ. Activated macrophages in experimental subretinal neovascularization. *Ophthalmologica*. 1990;200:39–44.
21. Sakurai E, Anand A, Ambati BK, van Rooijen N, Ambati J. Macrophage depletion inhibits experimental choroidal neovascularization. *Invest Ophthalmol Vis Sci*. 2003;44:3578–3585.
22. Van Rooijen N, Sanders A. Liposome mediated depletion of macrophages: mechanism of action, preparation of liposomes and applications. *J Immunol Methods*. 1994;174:83–93.
23. Nishihara H, Kondo M, Ishikawa K, et al. Focal macular electroretinograms in eyes with wet-type age-related macular degeneration. *Invest Ophthalmol Vis Sci*. 2008;49:3121–3125.
24. Curcio CA, Medeiros NE, Millican CL. Photoreceptor loss in age-related macular degeneration. *Invest Ophthalmol Vis Sci*. 1996;37:1236–1249.
25. Lewis GP, Fisher SK. Up-regulation of glial fibrillary acidic protein in response to retinal injury: its potential role in glial remodeling and a comparison to vimentin expression. *Int Rev Cytol*. 2003;230:263–290.
26. Soubrane G, Cohen SY, Delayre T, et al. Basic fibroblast growth factor experimentally induced choroidal angiogenesis in the minipig. *Curr Eye Res*. 1994;13:183–195.
27. Schwesinger C, Yee C, Rohan RM, et al. Intrachoroidal neovascularization in transgenic mice overexpressing vascular endothelial growth factor in the retinal pigment epithelium. *Am J Pathol*. 2001;158:1161–1172.
28. Heckenlively JR, Hawes NL, Friedlander M, et al. Mouse model of subretinal neovascularization with choroidal anastomosis. *Retina*. 2003;23:518–522.
29. Li C, Huang Z, Kingsley R, et al. Biochemical alterations in the retinas of very low-density lipoprotein receptor knockout mice: an animal model of retinal angiomatous proliferation. *Arch Ophthalmol*. 2007;125:795–803.
30. Chen Y, Hu Y, Lu K, Flannery JG, Ma JX. Very low density lipoprotein receptor, a negative regulator of the wnt signaling pathway and choroidal neovascularization. *J Biol Chem*. 2007;282:34420–34428.
31. Marticorena J, Di Leva V, Cennamo GL, de Crecchio G. Retinal angiomatous proliferation. *Curr Drug Targets*. 2011;12:199–205.
32. Blaauwgeers HG, Holtkamp GM, Rutten H, et al. Polarized vascular endothelial growth factor secretion by human retinal pigment epithelium and localization of vascular endothelial growth factor receptors on the inner choriocapillaris. Evidence for a trophic paracrine relation. *Am J Pathol*. 1999;155:421–428.
33. Rohrer B, Long Q, Coughlin B, et al. A targeted inhibitor of the alternative complement pathway reduces angiogenesis in a mouse model of age-related macular degeneration. *Invest Ophthalmol Vis Sci*. 2009;50:3056–3064.
34. Zipfel PF, Lauer N, Skerka C. The role of complement in AMD. *Adv Exp Med Biol*. 2010;703:9–24.
35. Jones A, Kumar S, Zhang N, et al. Increased expression of multifunctional serine protease, HTRA1, in retinal pigment epithelium induces polypoidal choroidal vasculopathy in mice. *Proc Natl Acad Sci U S A*. 2011;108:14578–14583.
36. Deangelis MM, Ji F, Adams S, et al. Alleles in the HtrA serine peptidase 1 gene alter the risk of neovascular age-related macular degeneration. *Ophthalmology*. 2008;115:1209–1215.e7.

Investigative Ophthalmology & Visual Science